Studies of LaAlO$_3${100} surfaces using RHEED and REM I: twins, steps and dislocations

Z.L. Wang *, A.J. Shapiro

National Institute of Standards and Technology, Bldg. 223, Gaithersburg, MD 20899, USA

Abstract

Lanthanum-aluminate (LaAlO$_3$) is one of the optimum substrates for epitaxial growth of YBa$_2$Cu$_3$O$_{7-x}$ thin films. In this paper, the structures of the {100} surfaces of annealed LaAlO$_3$ are studied using reflection electron microscopy (REM). The importance of substrate steps on the growth of defects in the film is shown. It has been found that a {010} twin boundary is normally terminated with a ⟨001⟩ step at the surface. Dislocations are not observed in the flat surface areas but occur at the twin boundaries that intersects the {100} surface. The observed dislocation is screw-type with Burgers vector a⟨100⟩. Numerous [010] and [001] "sawtooth" steps have been observed, and they are believed to be the lowest surface energy steps. It is suggested that the {100} surfaces are terminated entirely with either the La-O layer or the Al-O layer, but not a mixture of both. The miscut angle and the heights of surface steps are measured using the mirror imaging technique. Finally, the effect of surface contaminants on the growth of surface steps is shown, and a growth mechanism is proposed.

1. Introduction

In epitaxial crystal growth, the substrate should meet the following specifications in order to grow high-quality films. First, the lattice constants of the substrates should be closely matched to those of the films, so that the density of interfacial dislocations is minimized. Second, the substrate should not have phase transformations which create microtwins. Finally, only a minimal chemical reaction can be toler-

ated in the interface regions between the substrate and the film.

In epitaxial growth of high-temperature superconductor thin films, lanthanum-aluminate (LaAlO$_3$) is one of the optimum candidates for substrates [1,2]. The small lattice mismatch (< 2%) between LaAlO$_3$ and YBa$_2$Cu$_3$O$_{7-x}$ allows high-quality c-axis oriented superconducting thin films to be grown on the (100) surface of the substrate. Since the melting point of LaAlO$_3$ is about 2180°C, the interfacial reaction can be minimized under normal growth conditions.

In general, it is believed that the nucleation and growth of thin films are strongly affected by the structures of the substrate surfaces, such as steps and dislocations. However, few studies have been made

---
* Corresponding author. Present address: School of Materials Science and Engineering, Georgia Institute of Technology, Atlanta, GA 30332-0245, USA. Fax: +1 404 853 9140. E-mail: zwang@enh.nist.gov.

on the surface structures of LaAlO$_3$. In order to fully understand the effect of substrate surfaces on the growth of thin films, a series of studies has been

carried out. We have observed the direct relationship between the growth of columnar defects in YBa$_2$Cu$_3$O$_{7-x}$, which result from the steps on the
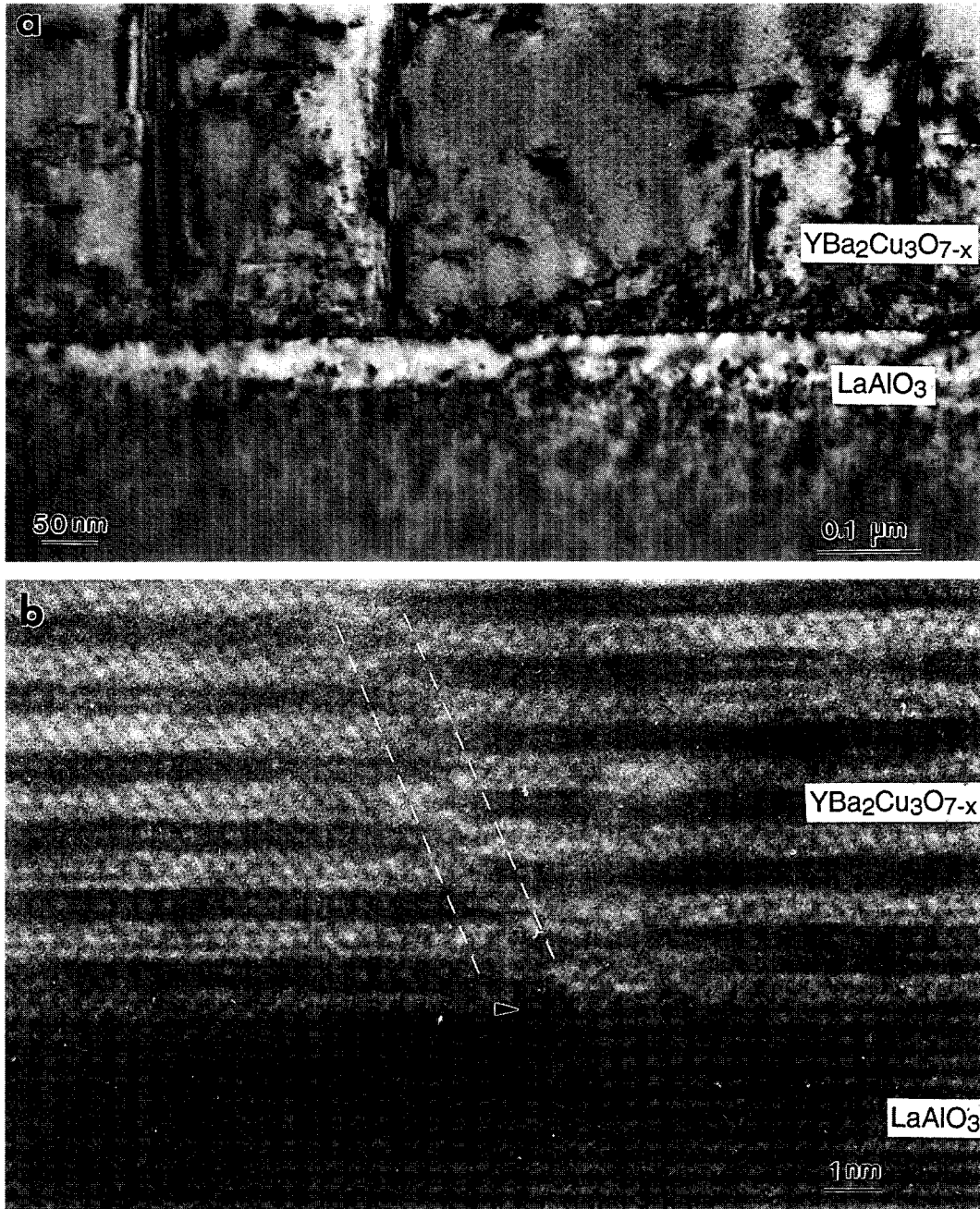

Fig. 1. (a) Low-magnification cross-section TEM image of YBa$_2$Cu$_3$O$_{7-x}$ film grown on LaAlO$_3${001} substrate, exhibiting columnar defects grown from the interface. (b) Cross-section high-resolution TEM image of YBa$_2$Cu$_3$O$_{7-x}$–LaAlO$_3$ interface showing a defect produced by a substrate step.

surfaces of $LaAlO_3$ substrates [2–5]. The present study is to examine the microstructures of the substrate surface. The reconstruction of the $LaAlO_3(100)$ surface will be reported separately [6].

Reflection electron microscopy is a powerful technique for imaging step structures of crystals [7,8]. This technique has been applied to study the domain structures of bulk $BaTiO_3(100)$ surfaces [9]. $LaAlO_3(110)$ has been studied with REM [10], and the surface shows rough structures and high-step terraces. In this paper, the {100} surfaces of $LaAlO_3$ are studied with REM. First, we will show some evidence which illustrates the importance of substrate steps in the growth of defects in $YBa_2Cu_3O_{7-x}$ thin films. Second, the twin structure, surface steps and dislocations are studied with REM. Third, the distribution of [010] and [001] surface steps on the (100) surface is determined, and its dependence on the miscut angle of the surface is demonstrated. The heights of surface steps are then measured using the mirror imaging technique. Finally, the effect of surface contaminants on the growth of surface steps is shown. Discussion regarding the formation of various observed features on the surface is presented.

2. Effect of surface steps on the growth of thin films

Before presenting the experimental results on the surface studies of $LaAlO_3$, it would be helpful to illustrate the influence of surface steps on the formation of defects in thin films. Fig. 1a shows a low magnification cross-section transmission electron microscopy (TEM) image of a c-axis oriented $YBa_2Cu_3O_{7-x}$ thin film grown on the (100) surface of $LaAlO_3$. Column defects are formed in the film and grown from the film–substrate interface. These defects are suitable for pinning vortices in $YBa_2Cu_3O_{7-x}$. Critical current density measurements of the $YBa_2Cu_3O_{7-x}$ thin film have shown an anomalous angular dependence of J_c [4]. A strong, broad, magnetic field direction-dependent peak in critical current density J_c is observed when the magnetic field is oriented between the c-axis (the film normal direction) and the $a–b$ plane (the substrate plane), orientations where flux pinning normally are not strong. The defects shown in Fig. 1a were found to be oriented perpendicular or nearly

perpendicular to the substrate surface, thus accounting for the observed anomalous pinning and high J_c with a magnetic field oriented at non-symmetry directions near the c-axis of the $YBa_2Cu_3O_{7-x}$ film [4,11]. Numerous stacking faults in the $a–b$ plane are also produced by the columnar defects, which can be effective flux pinners [12].

The substrate used to grow the film was a miscut $LaAlO_3(100)$ surface. It is thus expected that the film might contain highly oriented internal growth defects, induced by the steps on the substrate surface. Fig. 1b shows a (001) interface cross-section high-resolution transmission electron microscopy (HRTEM) image of the film and the substrate. The beam direction is [100]. No apparent interface reaction is seen. The columnar defect is apparently initiated at a substrate step. It is thus expected that a proper control of the density of the surface steps may affect the density of columnar defects, making it possible to optimize the critical current density when the magnetic field direction is between the c-axis and the $a–b$ plane of $YBa_2Cu_3O_{7-x}$ [3].

The example shown in Fig. 1 illustrates the importance of surface steps on the growth of thin films. This paper, therefore, is dedicated to the study of the structures of the $LaAlO_3(100)$ surface.

3. Experimental method and crystal structure

REM experiments were carried out in transmission electron microscopes under vacuum conditions of 10^{-6} to 10^{-7} Torr. The REM images were recorded with Philips EM430 (300 kV) and Philips EM400T (120 kV) TEMs. The high-resolution REM (HR-REM) images were recorded at 300 kV in the Philips 430 TEM equipped with a Gatan 622 intensified high-resolution video camera.

In REM, the incident electrons strike the crystal surface at a glancing-angle of a few degrees. This is the geometry for reflection high-energy electron diffraction (RHEED). If the surface resonance conditions are satisfied, which means the intersection of the specularly reflected beam with the resonance parabola, the electrons will penetrate into the surface only a few atomic layers before being reflected back. Since the electron wavelength ($\lambda = 0.0037$ nm for 100 kV electrons) is much shorter than the dimensions of an atom, a small change in the atomic

arrangement will generate a large phase shift in the electron wave due to a difference in the path-length. Therefore, REM has high surface sensitivity and can be easily applied to image atomic steps on single crystal surfaces. A detailed introduction of REM techniques and associated applications can be found elsewhere [7,8].

The crystallographic data on $LaAlO_3$ have been given by Geller and Bala [13] and Berkstresser et al. [14]. $LaAlO_3$ is the distorted-perovskite structure with lattice constant $a = b = c = 0.3788$ nm and α

$= \beta = \gamma = 90.066°$. The structure is referred to a face-centered rhombohedral cell, in which the La^{3+} ion locates at (000), the Al^{3+} ion at $(\frac{1}{2}\frac{1}{2}\frac{1}{2})$, and the O^{2-} ions at the face-centers $\{\frac{1}{2}\frac{1}{2}0\}$.

For REM observations, bulk specimens were prepared by cutting $LaAlO_3$ single crystal sheets into pieces with dimensions of about $2.5 \times 1 \times 0.8$ mm. The (100) surface was mechanically polished before annealing. The polished sample was annealed at 1500°C for 20 h in air. The purpose of annealing is to smooth the morphology of the surface so that it
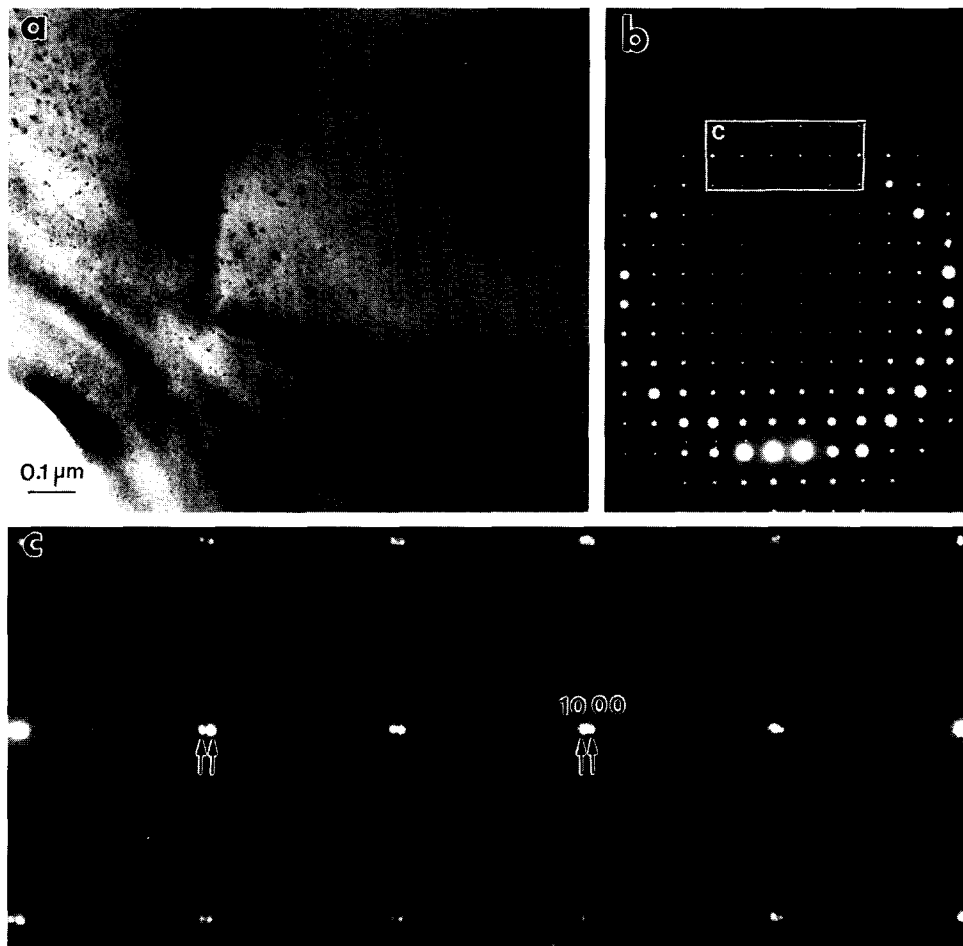

Fig. 2. (a) A TEM image showing the {100} twin planes in $LaAlO_3$. (b) A selected area diffraction pattern from the twinned region. The beam direction is close to [001]. (c) An enlargement of the reflection beams indicated in (b) showing the double splitting of the diffraction spots due to twinning.

will be suitable for REM studies. Sputtering may remove the surface contaminants before annealing, but contamination can be introduced during annealing in air. A $LaAlO_3$ bridge was made in order to support the crystal inside the furnace, so that the annealed crystal did not contact any other objects of different chemical compositions. The crystal and the bridge were enclosed by an α-alumina box during annealing.

4. Experimental results and analysis

4.1. Twinning of $LaAlO_3$

$LaAlO_3$ exhibits {100} twin structures. The (100) and (010) twin planes are clearly observed in TEM of a thin $LaAlO_3$ foil, as shown in Fig. 2a. However, the splitting of the diffraction spots is hardly seen when the crystal was oriented exactly along the [001]
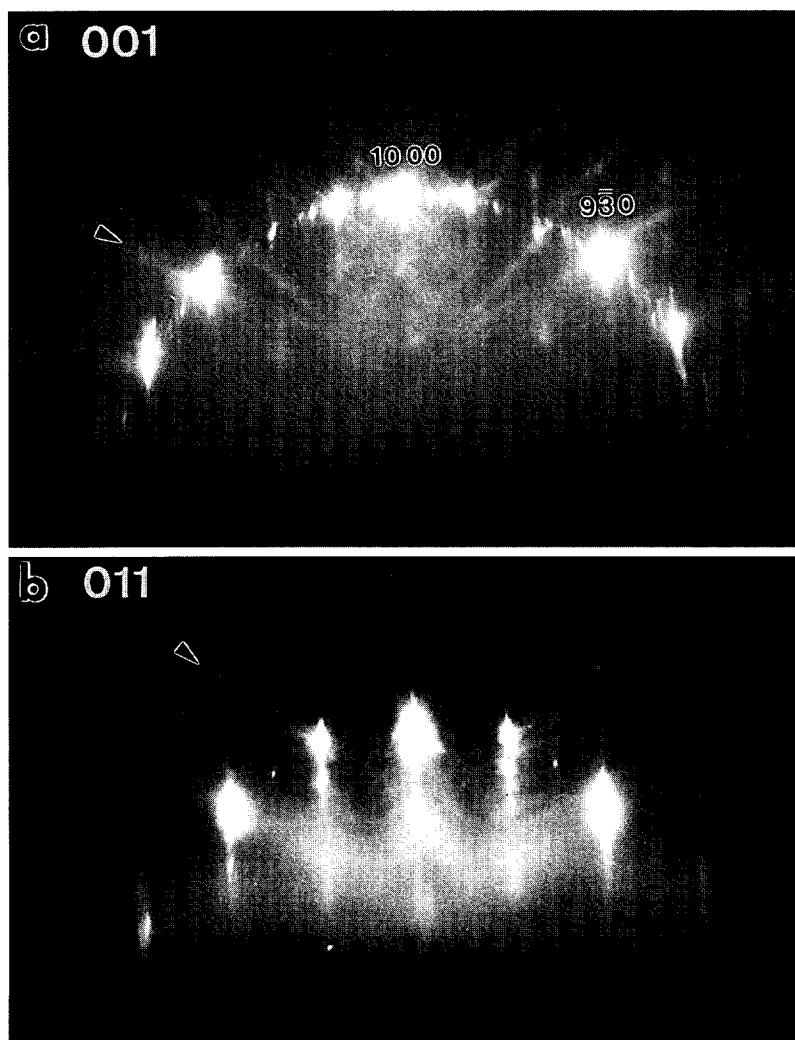

Fig. 3. (a) [001] and (b) [011] selected area RHEED patterns from an annealed $LaAlO_3$(100) surface. The parabolas are indicated by arrowheads.

zone axis due to the curvature of the Ewald sphere. The splitting is easier to see if the crystal is tilted slightly away from the [001] zone so that the Ewald sphere cuts through the higher index reflections. Fig. 2b shows a transmission electron diffraction pattern recorded under the (10 0 0) Bragg reflection condition. An enlargement of the pattern shows the spot splitting (Fig. 2c). The twin angle can be measured from the diffraction pattern as 0.18°. This observation will be useful in interpretation of the Bragg spot splitting in RHEED. The mechanism for forming twins in this material is given by Berkstresser et al. [14]. TEM studies of LaAlO₃ have been reported by Yagi et al. [15], who observed the anti-phase boundaries.

4.2. Twin planes and dislocations

Fig. 3 shows [001] and [011] RHEED patterns of the annealed LaAlO₃(100) surface. Two important features are seen. Some "extra" superlattice reflections are seen besides the Bragg reflections from the

bulk LaAlO₃. These superlattice reflections are equally spaced and are separated by $\frac{1}{5}$(010) of the bulk reflection. Further studies have shown that these superlattice reflections correspond to the formation of 5 × 5 reconstruction on the surface [6]. Second, parabola-shaped curves are seen in the background of the RHEED pattern. The formation of these parabolas will be described below. In this paper, we concentrate on the studies of twin boundaries, steps and dislocations of the LaAlO₃ surfaces. The studies of the 5 × 5 surface reconstruction are reported separately [6].

The continuous weak curves intersecting the Bragg beams are the so-called resonance parabolas and Kikuchi envelopes. For crystals containing no twins, one resonance and one Kikuchi envelope are usually associated with each reflected beam under the resonance condition [7], and both are separated by a small gap due to the crystal refraction effect. The Kikuchi envelope is formed by the electrons scattered within the bulk crystal, and it is associated with the symmetry of the crystal. The electrons scattered
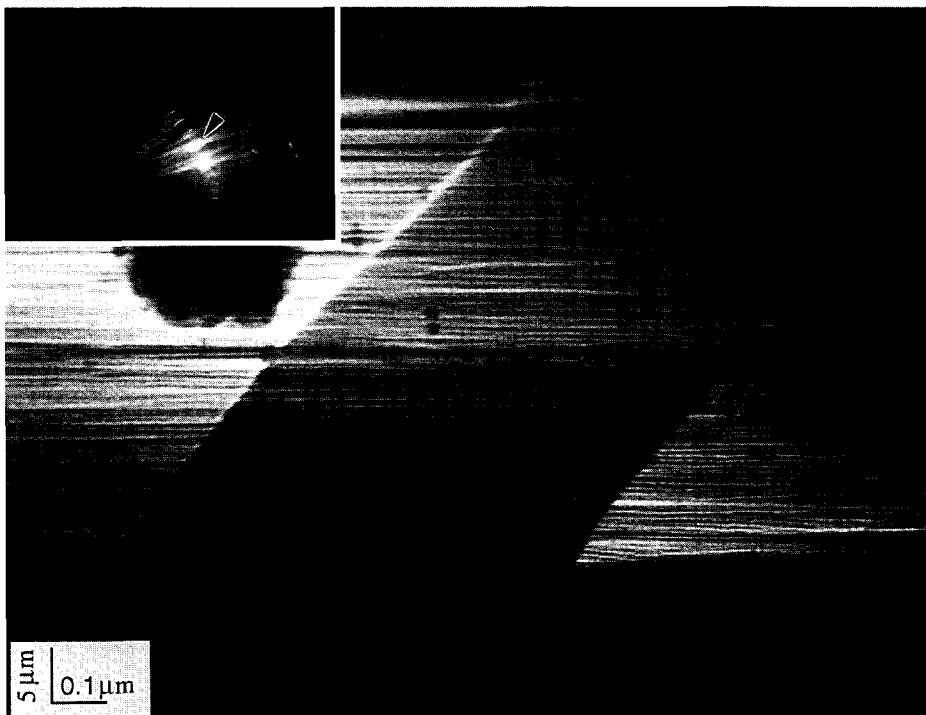

Fig. 4. A REM image recorded from the LaAlO₃(100) surface showing the (010) twins. Beam azimuth near [001]. The diffracting condition for recording the image is shown in inset. [001] steps may present at the twin boundaries.

by the bulk are refracted when they exit the crystal surface due to the effect of average crystal inner potential [16]. This pattern appears in RHEED regardless of the diffracting conditions. The resonance parabola is produced by the electrons scattered from the top few atomic layers [16,17], and this scattering is significant only under the resonance condition. In practice, electrons channeling along rows of atoms near the surface may "see" a potential that is different from the average potential of the crystal, resulting in a slightly larger refraction effect [16,18]. Hence the continuous parabola, generated by channeling electrons, is displaced relative to the straight Kikuchi lines, which arise from non-channeled electrons, and there is a gap between the parabola and the envelope of the straight Kikuchi lines. Thus, the resonance parabola and the Kikuchi envelope are produced by the surface and bulk scattering, respectively.

In RHEED, the excitation of surface resonance critically depends on diffracting conditions. It has been found that the resonance occurs only within an angular width smaller than 2 mrad [19]. If one of the

twin grains is oriented at the exact resonance condition, a pair of resonance parabola and Kikuchi envelope is seen. The other grain, however, is oriented at the non-resonance diffracting condition due to its rotation by the twin angle, resulting in the disappearance of the resonance parabola, but the Kikuchi envelope is still preserved because it comes from the scattering of the bulk. Therefore, a total of three curves in parabola-shape are associated with each Bragg reflected beam. This expected result has been observed experimentally (Fig. 3). In Fig. 3a, three continuous curves in parabola-shape are associated with each Bragg reflected beam, as indicated by arrowheads. Two of them are produced by the Kikuchi envelopes of the twinned crystals. The other one is the resonance parabola from one of the twinned crystals which is set at the resonance condition.

In Fig. 3b, four continuous curves in parabola-shape are associated with each Bragg beam. Two of them are the Kikuchi envelopes of the twinned crystals. The other two are the resonance parabolas of the twinned crystals, which are oriented to satisfy the resonance conditions simultaneously due to a slight
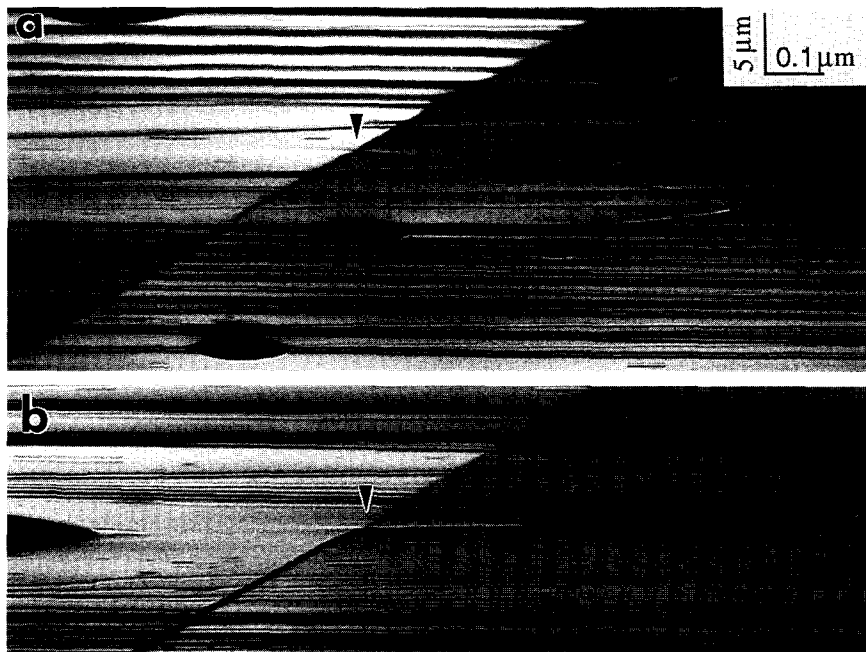

Fig. 5. REM images recorded from the LaAlO$_3$(100) surface, showing the (010) twins and screw-type dislocations associated with the twin boundaries. Beam azimuth near [001]. The images were recorded at 300 kV under the same diffracting conditions as for Fig. 4.

Fig. 6. REM images of the LaAlO$_3$(100) surface showing the [010] and [001] faceted steps and surface morphology. The images were recorded with the (10 0 0) specular reflection beam under the diffracting conditions shown in Fig. 3a. In (c) small islands and hollows are seen.

convergence of the incident beam across the illumination area. The entire surface is illuminated by a convergent beam, so that the incident angle of the electrons varies across the surface area.

In REM, the strain field produced by dislocations introduces strong contrast in the image. Fig. 4 shows a REM image of an annealed LaAlO$_3$(100) surface. Both ends of the (001) twinned grains are seen, but the contrast at the twin boundaries is reversal. The contrast reversal can be interpreted based on the diffraction contrast mechanism of REM. If the left-hand twin-boundary region is set at Bragg condition due to a strain modulation $R(r)$ and shows bright contrast, the right-hand twin boundary region must be out of Bragg condition due to an opposite lattice modulation $-R(r)$, resulting in dark contrast. The strain associated with the twin boundary may be introduced by the presence of dislocation at the boundary, as will be shown in Fig. 5.
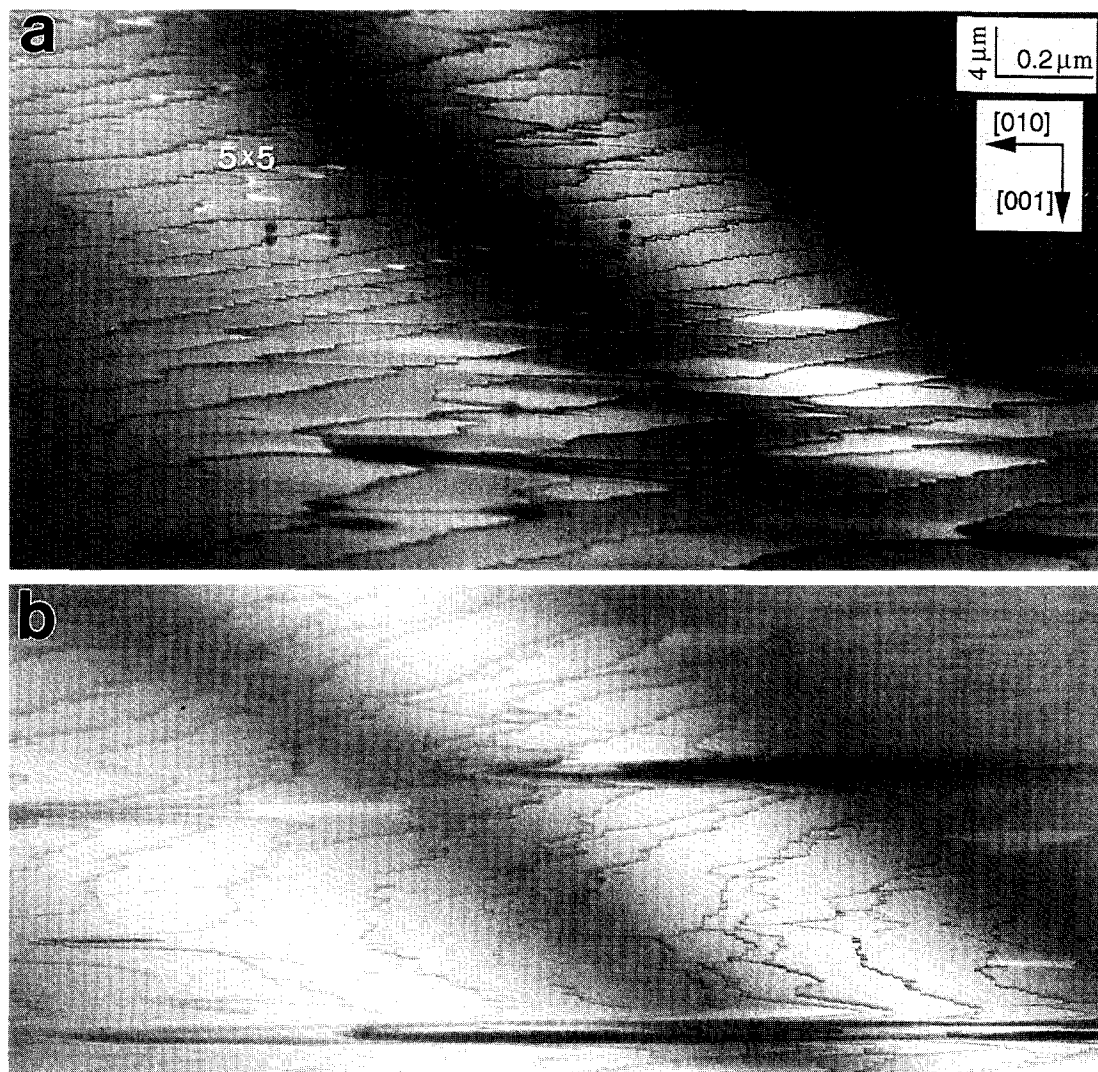
Another characteristic of REM is its high sensitiv-

Fig. 7. REM images of the LaAlO$_3$(100) surface showing the [010] and [001] faceted "sawtooth" steps. The surface is almost entirely covered by the 5×5 reconstruction. The images were recorded with the $(10\,0\,0)$ specular reflection beam under the diffracting conditions shown in Fig. 3a.

ity to surface emergent dislocations and steps. For annealed LaAlO$_3$(100), no dislocation is found in the flat surface areas. Dislocations, however, seem to be associated with twin boundaries, as shown in Fig. 5. The twin boundaries run from the upper-right corner to the lower-left corner in the image. The dislocations indicated by arrowheads are screw-type dislocations due to their association with surface steps. It is also seen that a surface step is present at the twin boundary. The displacement of the dislocation is confined in the (010) plane and is directly connected to a [001] step, thus the Burgers vector of the dislocation is probably a[100]. Based on the contrast, the height of the twin-boundary step is reduced to about half after it crosses the dislocation. Since the magnitude of dislocation Burgers vector is the size of the lattice constant, the height of the twin-boundary step is about twice the unit cell lattice constant.

4.3. ⟨100⟩ steps on the surface

Numerous surface steps were observed on the LaAlO$_3$(100) surfaces. Fig. 6a is a REM image recorded with the (10 0 0) specularly reflected beam under the diffracting conditions shown in Fig. 3a. [010] and [001] surface steps are seen. "Stair-type" [010] steps are observed in the area that shows

compiled steps with high density. Both down- and up-steps (with respect to the incident beam) are present. Large curved surface steps are seen in the REM image shown in Fig. 6b. But these curved steps are composed of small [010] and [001] faceted segments that have lengths between 10 and 80 nm.

The annealed (100) surface is normally flat. The surface has approached the thermal equilibrium structure after being annealed for 20 h at 1500°C. However, some small islands/vacancy terraces are occasionally seen in the REM image (Fig. 6c). This indicates that the rate at which the surface diffusion occurs may not be uniform across the entire specimen and may depend on the morphology of the surface.

The faceted [010] and [001] steps are the most common features seen on the (100) surface. Fig. 7a shows a REM image that exhibits the "sawtooth" steps on the surface. The non-uniform contrast across the entire image is produced by the converged beam illumination and the diffraction effect of the crystal. The sawtooth structure is formed by the [010] and [001] microfaceted steps. The width of the sawtooth can be as small as 10 nm. The REM image shows two distinct contrast regions. The regions which show brighter and darker contrast sometime share the same terrace, and there is no step between them.
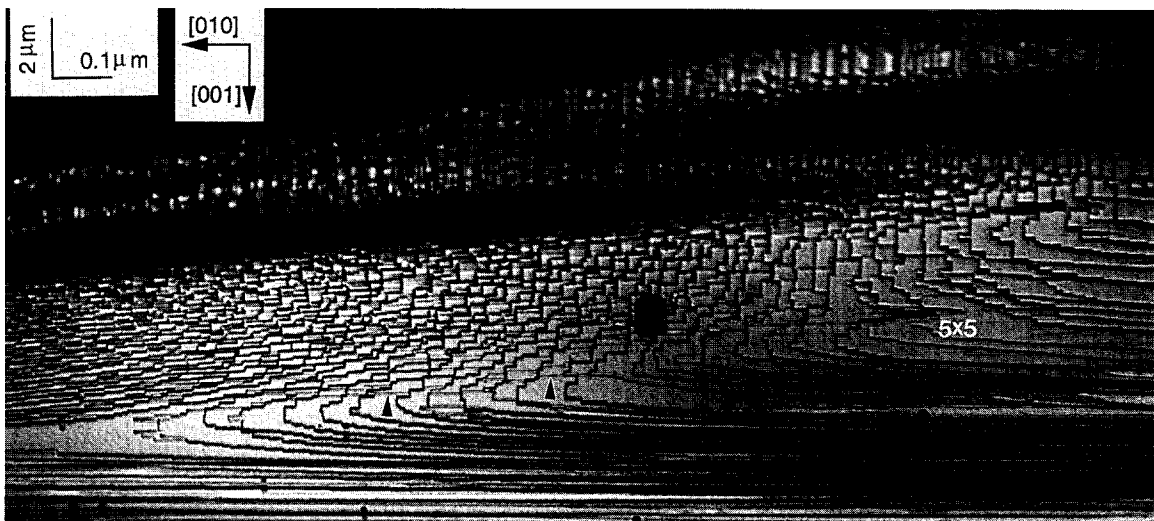

Fig. 8. A REM image of the LaAlO$_3$(100) surface showing the distribution of [010] and [001] faceted steps at a surface region where many steps are exhibited. The entire surface displays the 5 × 5 reconstruction. The images were recorded with the (10 0 0) specular reflection beam under the diffracting conditions shown in Fig. 3a.

As shown by the RHEED pattern in Fig. 3a, surface reconstruction is observed. In the REM image, the 5 × 5 reconstructed area shows darker contrast due to the reduction of the (10 0 0) reflected beam intensity as the result of exciting the superlattice reflections. The unreconstructed surface areas show brighter contrast. Some of the surface areas are completely covered by the reconstructed surface layer. But the formation of [010] and [001] steps is unaffected. The faceted steps are seen almost everywhere on the surface (Fig. 7b).

Fig. 8 shows a REM image of the (100) surface, which is completely covered by the 5 × 5 reconstruction layer. Many densely distributed [001] and [010] facets are seen. Some smaller steps (indicated by arrowheads), whose height is half or one third of the larger steps, are also seen.

As a summary, the [001] and [010] faceted steps are commonly seen on the annealed (100) surface of LaAlO$_3$. When the specimen was annealed at 1500°C, the surface atoms tend to move to the positions where they are expected to have the lowest energy. Our observations show that the $\langle 100 \rangle$ steps preserve the lowest energy in comparison to steps along any other direction.

4.4. Measurements of surface miscut angle and step height

Measuring step height in REM is not always possible, particularly for steps a few atoms high. The phase contrast produced by atom-high steps depends sensitively on objective lens focus, crystal orientation, beam coherence, resonance and diffracting conditions and the step height. It is usually difficult to measure the absolute heights of steps directly from the image contrast. In epitaxial growth of thin films, LaAlO$_3${100} substrates are usually cut from a bulk crystal. Since LaAlO$_3$ is rhombohedral with $\alpha = 90.0667°$, it is very possible that the {100} surfaces are miscut at a small angle. Therefore, the density of surface steps may critically depend on the miscut of the surface. In this section, we use a method introduced by Kim and Hsu [20] to measure the step height.

In REM, an object erecting on the crystal surface shows two images similar to the image pair formed with a planar mirror. An erect image is formed by
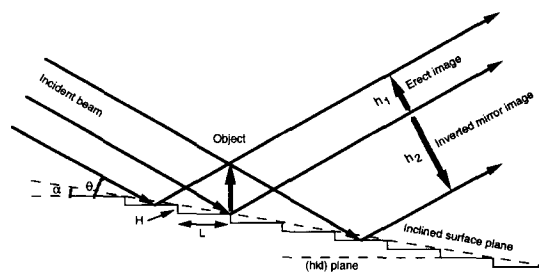

Fig. 9. A schematic ray diagram showing the formation of a non-symmetric inverted mirror image of an erect object on the surface, where the surface steps are assumed to be the same height and equally spaced on the surface.

the electrons that are reflected from the surface area before the object. The inverted mirror image is formed by the electrons that are reflected by the surface area after the object. These electrons interact with the object first before being reflected by the surface. If the surface plane is the (hkl) reflection plane of the crystal and it is perfectly flat without steps, the two images are identical but inverted with respect to each other. However, the images are not symmetric if there are steps on the surface. Fig. 9 shows a schematic ray diagram for the formation of the paired images. For simplicity, we assume that the surface steps are the same height and are equally spaced in the direction nearly perpendicular to the beam azimuth. The surface plane is assumed to be the (hkl) crystal plane for generating the $n(hkl)$ specularly reflected beam which was used to record the REM image. The angle between the surface plane and the (hkl) crystal plane is defined as the miscut angle. For glancing angle incidence and if the object is standing normal to the surface, the miscut angle of the surface [20] is

$$\alpha \approx \theta \frac{h_2 - h_1}{h_2 + h_1}, \qquad (1)$$

where θ is the glancing incident angle of the beam and can be measured directly from the RHEED pattern, h_1 and h_2 are the heights of the erect and inverted object images, respectively, which can be measured from the REM image. The step height is

$$H \approx L\alpha, \qquad (2)$$

where L is the average distance between two adjacent surface steps in the surface plane. Eqs. (1) and

(2) have been applied to measure the miscut angle of the surface and the step height.

Fig. 10 shows a REM image of an object on the LaAlO$_3$(100) surface. The paired images are similar to the paired "bird wings". The inverted image is longer (or shorter) than the erect image, indicating the steps are down (or up) steps. From the RHEED pattern shown in Fig. 3a, we have $\theta = 48.8$ mrad. The miscut angle of the surface is $\alpha \approx 0.19° \pm 0.01°$; the average step height is thus $H = 1.8 \pm 0.2$ nm, where the uncertainty comes from the inaccuracy in measurements of h_1, h_2 and θ. The measurement from two other REM images shows the average step height is 1.0 ± 0.1 nm. It must be pointed out that the measurement only gives an average value of the step heights.

We now consider the restriction of the mirror-imaging technique for measuring step height. In Eq. (1), since $|h_2 - h_1| < h_2 + h_1$, thus the maximum miscut angle that can be measured using this technique is $\alpha_{max} \approx \theta$. The maximum step height which can be measured by the technique is $H_{max} = L\theta$.

It must also be pointed out, however, that the above analysis is based on an assumption that the erect object is standing vertically on the surface. As pointed out by Kim and Hsu [20], the measured step height can significantly deviate from the actual step height if the object is declined with respect to the incident beam direction. It is thus strongly suggested that the step height should be measured from the mirror-images of a few different objects. The consistency between the measured data must be examined before a reasonable step height is given.

4.5. Contaminants and surface step morphology

As pointed out in Section 4.2, protrusion contaminants are seen on the surface. In order to determine the nature of the contaminants, a specimen used for REM imaging was analyzed in a scanning electron microscope (SEM), JEOL JXA 840 SEM, which was equipped with an ultra-thin-widow energy dispersive X-ray spectrometer (EDS) that is capable of detecting both light and heavy elements. The analyzed
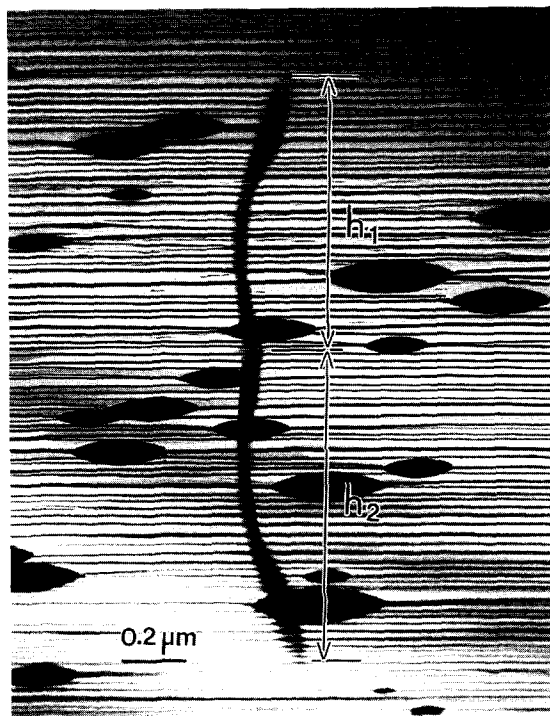

Fig. 10. A REM image of the LaAlO$_3$(100) surface showing the paired images of an erect object on the surface. This image is used to measure the height of surface steps (see text). The image was recorded using the (10 0 0) specular reflected beam under the diffracting conditions shown in Fig. 3a.

results showed that the particles are composed of mainly silicon and oxygen and a small portion of La. The possible sources for forming the Si–La–O compound will be discussed in Section 5.3.

No silicon or other non La–Al–O elements were detected by EDS on the surface areas where there are no Si–La–O particles. Therefore, the surface areas without particles are not contaminated by Si–O or any other elements, beyond the detection limit of EDS which is about 1%.

In REM, the image is shrunk along the beam direction due to the foreshortening effect. The foreshortening factor is $1/\theta$, which is 20, 40 or 50 in our experiments depending on the accelerating voltage and the reflection index of the beam used for imaging. The particles distributed on a large surface area along the beam direction will be projected onto a much smaller image plane. Thus, the density of the particles in the REM image appears to be much higher than that observed in the SEM images.

For most cases, the surface step structures are undisturbed by the presence of the Si–La–O protrusions. This result has been seen in the images shown in the last few sections. However, it has been occasionally found that the morphology of surface steps can be drastically affected by the presence of the particles. Fig. 11 shows a REM image of LaAlO$_3$(100), in which the Si–La–O particles are almost aligned. Three features are seen. First, the particles are almost aligned along [001], the direction in which the beam strikes the surface. The surface structure is nearly symmetric on the two sides of the particle line. Second, the particles are distributed on a "long-island" which is relatively flatter and higher than the neighboring regions. Third, down steps are seen on both sides of the particles. At distances far away from the particles, the surface is covered by the [010] steps, which are frequently seen in most REM images.

Fig. 12 shows several more features in another
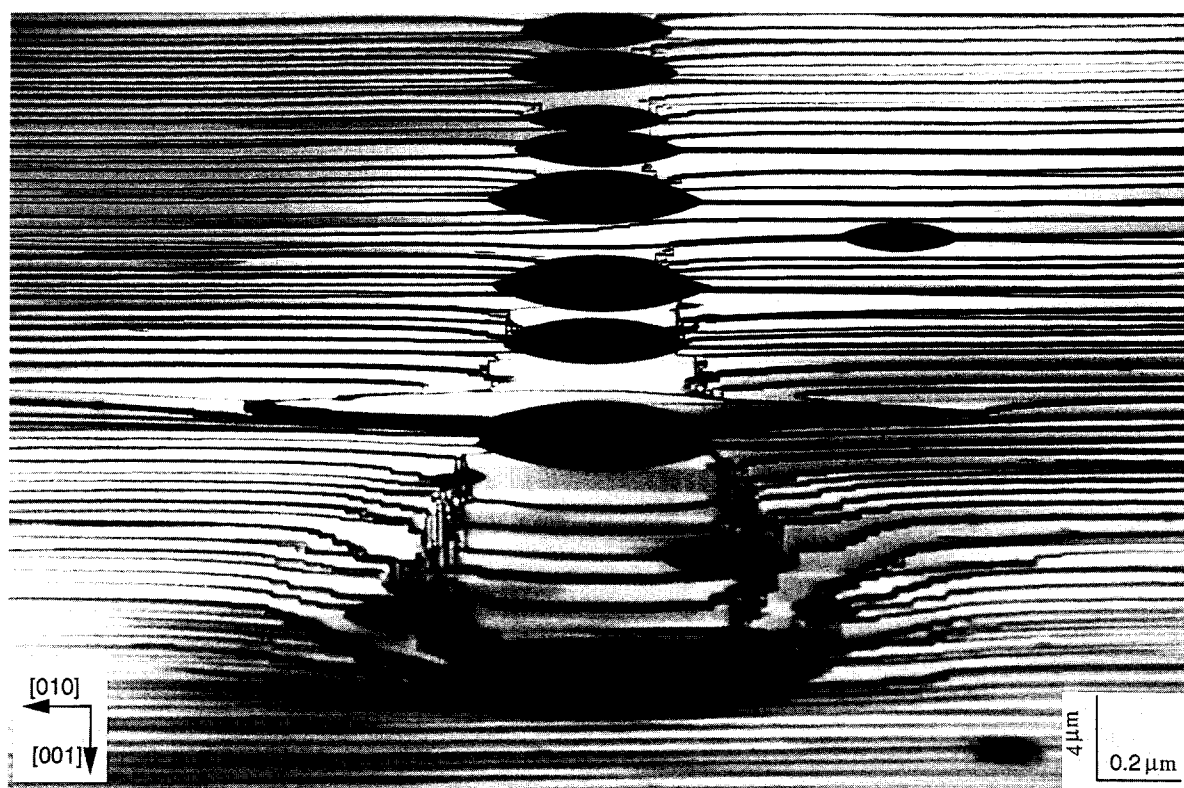
Fig. 11. A REM image of the LaAlO$_3$(100) surface showing the effect of the Si–La–O particles on the formation of surface steps. The image was recorded using the (10 0 0) specular reflected beam under the diffracting conditions shown in Fig. 3a.

REM image of the (100) surface. Symbols 1 to 6 indicate some larger Si–La–O particles seen on the surface. Each particle is surrounded by down steps, and the step configuration is approximately symmetric on the two sides of the particle. Each particle sits on the top of the step terraces (or island). Particles 1 and 3 are surrounded by down steps, which are actually "circular" in shape if the foreshortening effect is considered. The steps are [010] and [001]. There are smaller size particles distributed between particles 1 and 2, 2 and 3, 3 and 4, and 4 and 5. The steps symmetrically distributed around particle 1 are almost unaffected by the nearby particles due to the large size of the particle and the large distance away from other particles. The formation of these features will be discussed in Section 5.2.

The REM images shown in Figs. 11 and 12 have clearly demonstrated the effect of surface contaminants on the growth of surface steps. However, it must be pointed out that these structures are rare.

5. Discussion

5.1. Surface steps

The experimental observations presented above have shown that the formation of [001] and [010] faceted steps on the (100) surface of $LaAlO_3$ is a very common feature. This can be easily understood because (100) is the most densely compacted surface, in which the density of atoms is larger than that

Fig. 12. A REM image of the $LaAlO_3(100)$ surface showing the effect of the Si–La–O particles on the formation of surface steps. The image was recorded using the (10 0 0) specular reflected beam under the diffracting conditions shown in Fig. 3a. This image is a match of two images recorded under different focusing in order to view the entire region clearly. The sharp line across particle 3 is the match line, the contrast variation across which is purely a photographic effect and has nothing to do with the structure of the surface. Particles 1–6 are the surface contaminants. Particle 7 is a fracture fragment standing on the surface.

in any other crystallographic planes. Thus, the (100) surface exhibits the lowest surface energy.

Dislocations were observed at the twin boundaries, but not on the twin-free surface areas. This indicates that the stress built in the crystal is effectively released by the twin planes. Early studies of Yagi et al. [15] have shown that anti-phase boundaries always terminate at dislocations, and additional lattice mismatch at the anti-phase boundary can produce residual diffraction contrast in the image. As noted in Fig. 3b, two weak kinetically forbidden reflections are observed. These reflections should not appear in the pattern unless there is a superstructure of periodicity $2a$ perpendicular to the (100) surface. These superlattice reflections have also been observed in our transmission electron diffraction patterns of a thin $LaAlO_3$ crystal oriented along [110], but no additional spots appear in the [001] pattern. Therefore, the weak reflections observed in Fig. 3b are bulk effect rather than surface, corresponding to the formation of a single directional superstructure. This structure may be responsible for the formation of the anti-phase boundary observed by Yagi et al. [15].

Since $LaAlO_3$ has the face-centered rhombohedral structure, as described in Section 3, the (100) surface can be terminated with either a La–O layer or an Al–O layer. Thus, there are three possible configurations for forming a [001] or [010] step on the (100) surface. (a) Both the upper and lower terraces of the step are terminated with the La–O layer, and the step height is a multiple of the lattice constant. (b) Both the upper and lower terraces of the step are terminated with the Al–O layer, and the step height is again a multiple of the lattice constant. (c) The upper and lower surface terraces next to the step are terminated with the La–O layer and the Al–O layer, respectively. The step height is $(n + \frac{1}{2})a$, where $n = 0, 1, \ldots$. These configurations are schematically shown in Fig. 13, where, for simplification, only the atoms located on the top surface are shown. If configuration (c) were the case, the upper and lower terraces next to the step would show different contrast because of the difference in scattering powers between La (atomic number $Z = 57$) and Al ($Z = 13$), and the regions which show distinct difference in contrast would be separated by the surface step. However, this result was not observed
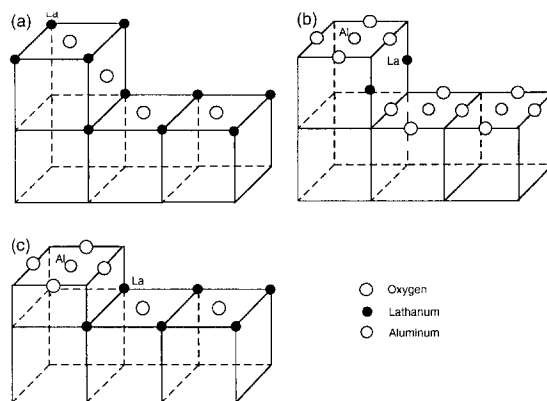

Fig. 13. Schematic diagrams showing the three possible configurations for forming a surface step on the (100) surface of $LaAlO_3$.

experimentally. The two types of contrast seen in the REM image, as shown in Fig. 7a for example, are due to surface reconstruction [6]. If configurations (a) and (b) both occur, a difference in contrast should also be seen due to the larger scattering power of La than that of Al, and the regions which show distinct difference in contrast must be separated by surface steps. This expected result again has not been observed experimentally. Therefore, the termination of the (100) surface must be produced solely by the La–O layer or the Al–O layer, but cannot be a mixture of the two. This is consistent with the result of $SrTiO_3(100)$, which is terminated only with a Ti–O layer when annealed in an oxygen atmosphere [21]. The step height is an integer of the lattice constant, in agreement with the 0.4 nm steps observed on the annealed $SrTiO_3(001)$ surface [22]. The precise determination of the surface termination is probably beyond the limitation of REM technique. However, it must be pointed out that the surface termination can, in some cases, be determined by REM if the termination-sensitive beam-damage effect is present, such as the cleavage $(01\bar{1}1)$ and $(01\bar{1}2)$ surfaces of α-Al_2O_3 [23–25]. Recent cross-section high-resolution electron microscopy studies have shown that $LaAlO_3\{100\}$ is terminated with La–O [26]. It must also be pointed out that the discussion given above is purely based on the clean surface structure. The effects of surface reconstruction and adsorption are not considered.

As illustrated in Fig. 1, the presence of steps on the substrate surface can greatly change the growth
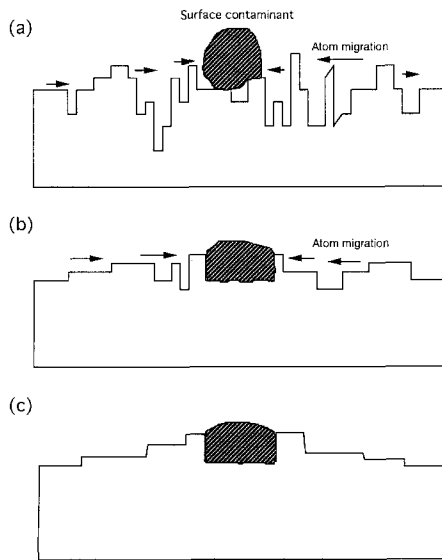
(a)

(b)

(c)

Fig. 14. A schematic diagram showing the nucleation and growth of surface steps around the Si–La–O contaminant during annealing.

behavior of thin films, possibly due to production of screw-type dislocations at the interfacial region. Normally, the annealed substrate surface is much smoother than the as-polished surfaces. Thus, it is expected that a better quality of film may be grown on the annealed substrate, provided there is no surface adsorption.

5.2. Formation of steps around Si–La–O particles

In Figs. 11 and 12, nearly symmetric, stair-type steps are grown around a Si–La–O particle. A possible growth mechanism for the formation of steps is given in Fig. 14. In general, an as-polished surface is composed of many up and down steps, kinks and ledges, as schematically shown in Fig. 14a. A contaminant locates on the surface. When the annealing temperature is sufficiently high, the surface atoms start to migrate from ledges to vacancies, and the surface starts to become flat toward low surface energy state (Fig. 14b). The presence of the Si–La–O particle on the surface, however, may create some nucleation sites at the intersection of its surface with the LaAlO$_3$ surface, to where the surface atoms tend to migrate. We assume here that the sites near the contaminant have lower surface energy. Thus the steps around the Si–La–O particle start to grow due

to the migration of the atoms toward the particle. After a long diffusion time, the atoms from the lower terraces tend to move to higher terraces that are located closer to the Si–La–O particle, and the atoms located further away from the Si–La–O particle may tend to move toward the lower terraces around the Si–La–O particle, resulting in the growth of stair-type down steps around the Si–La–O particle (Fig. 14c). If the surface diffusion is isotropic around the Si–La–O particle, "circular" stair-type steps are finally formed. The fact that [001] and [010] have the lowest step energy allows facets to form on the grown steps.

If two Si–La–O particles are located at a short distance apart, the lower terraces around them will meet if the growth time is long enough. Such a process can extend to several particles on the surface, resulting in the formation of "long-island" type structure, as seen in Figs. 11 and 12.

The long-island structure seen in Figs. 11 and 12 is parallel to the [001] direction (the incident beam direction). The particles appear to align along [001]. This alignment is enhanced by the foreshortening effect, which effectively reduces the distance between the particles in the REM image. The long-island structure also exists along [010] which is perpendicular to the incident beam. The alignment of particles parallel to [010], however, is not enhanced by the foreshortening effect, and the particle separation may be far enough that observation is difficult. The beam illumination circle can only light up a few of the aligned particles which are assumed to be separated by about 1 μm.

5.3. Formation of the Si–La–O particles

There are three possible sources for forming the Si–La–O particles: (1) residual polishing powders left on the surface before the annealing experiment, (2) contaminants from the oven during annealing treatment, and (3) segregation of impurity elements at the surface. The presence of La in the contaminants indicates that the particle is a reaction product of La with Si and O. Lanthanum may be reduced from LaAlO$_3$, and oxygen can come from air, but Si must be coming from other sources. The residual SiO$_2$ polishing powder is a very possible source, which tends to initiate the growth shown in Figs. 11

and 12. However, the surface regions which display the microstructure shown in Figs. 11 and 12 can only been found occasionally. The majority areas of the surface exhibit the structures as shown in Figs. 7, 8 and 10. The formation of Si–La–O particles during annealing due to oven contamination cannot be ruled out. The segregation of Si at the surface due to annealing is also expected to contribute a small amount to the formation of the Si–La–O product. It has been observed that small islands are formed on $SrTiO_3$(001) after being annealed at 1300°C in ultra-high vacuum [21]. The segregation of Sr at the surface was also observed.

The melting point of the Si–La–O particles is probably lower than the annealing temperature (1500°C). The particles were partially melted during annealing. Thus, the particles are affiliated on the surface in a "wet-coating" form. The surface tension kept the particles button-shaped as seen in the REM images.

6. Conclusions

In this paper, the importance of substrate steps on the growth of thin films has been shown. Defects can be directly initiated from the substrate steps. The {100} surfaces of annealed $LaAlO_3$ are studied using reflection electron microscopy (REM). The {100} twin planes and surface emergent dislocations are imaged. It has been found that a ⟨001⟩ step is normally associated with a {010} twin boundary. No dislocations were observed in the flat surface area but dislocations were found at the twin plane that intersects the {100} surface. The dislocation is screw-type possibly with Burgers vector $a⟨100⟩$. Numerous [010] and [001] surface steps are observed on the (100) surface. The length of the [010] and [001] steps can be as short as 10 nm. It is concluded that the ⟨100⟩ steps preserve the lowest surface energy in comparison to steps along other directions. ⟨100⟩ steps have been found to be the fastest growth directions.

The miscut angle of the substrate and step heights are measured using the mirror imaging technique in REM. The dependence of step morphology on the miscut of the surface has been illustrated. It is suggested that the (100) surface is entirely terminated

with the La–O layer or the Al–O layer, but not by the mixture of the two. The effect of surface contaminants (Si–La–O) on the growth of surface steps is shown. A growth mechanism is proposed to interpret the experimental observations. Finally, surface reconstruction on {100} has been observed with RHEED and REM, and the detailed study of this structure will be reported separately [6].

Acknowledgements

References

[1] R.K. Simon, C.E. Platt, K.P. Daly, A.E. Lee and M.K. Wagner, Appl. Phys. Lett. 53 (1988) 2677.

[2] D.H. Lowndes, X.Y. Zheng, S. Zhu, J.D. Budai and R.J. Warmack, Appl. Phys. Lett. 17 (1992) 852.

[3] Z.L. Wang, D.K. Christen, C.E. Klabunde, D.M. Kroeger, D.H. Lowndes and D.P. Norton, in: Proc. of 52nd Annu. Meeting of Microscopy Soc. of America, New Orleans (San Francisco, CA, 1994) p. 790.

[4] D.H. Lowndes, Z.L. Wang, D.K. Christen, C.E. Klabunde, D.M. Kroeger and D.P. Norton, in preparation.

[5] Z.L. Wang, D.K. Christen, C.E. Klabunde, D.M. Kroeger, D.H. Lowndes, D.P. Norton and A.J. Shapiro, in preparation.

[6] Z.L. Wang and A.J. Shapiro, Surf. Sci. 328 (1995) 159.

[7] Z.L. Wang, Rep. Prog. Phys. 56 (1993) 997.

[8] K. Yagi, Surf. Sci. Rep. 17 (1993) 305.

[9] F. Tsai and J.M. Cowley, Ultramicroscopy 45 (1992) 43.

[10] Z.L. Wang and A.J. Shapiro, in: Evolution of Thin-Film and Surface Structure and Morphology, Proc. of MRS, Eds. B.G. Demczyk, E. Garfunkel, B.M. Clemens, E.D. Williams and J.J. Cuomo (Materials Research Soc., Pittsburgh, PA, 1995).

[11] D.K. Christen, J.R. Thompson, H.R. Kerchner, B.C. Sales, B.C. Chakoumakos, L. Civale, A.D. Marwick and F. Holtzberg, in: American Institute of Physics Conf. Proc., Vol. 273, Superconductivity and its Applications, Eds. H.S. Kwok, D.T. Shaw and M.J. Naughton (Am. Inst. Phys., New York, 1992) p. 24.

[12] Z.L. Wang, A. Goyal and D.M. Kroeger, Phys. Rev. B 47 (1993) 5373.

[13] S. Geller and V.B. Bala, Acta Cryst. 9 (1956) 1019.

[14] G.W. Berkstresser, A.J. Valentino and C.D. Brandle, J. Cryst. Growth 109 (1991) 467.

[15] K. Yagi, N. Yamamoto and G. Honjo, Proc. 34th Annu. Meeting, Electron Microsc. Soc. Am., Ed. G.W. Bailey (Claitor, 1976) p. 626.

[16] L.M. Peng and J.M. Cowley, J. Electron Microsc. Tech. 6 (1987) 43.

[17] G. Lehmpfuhl and W.C.T Dowell, Acta Cryst. A 42 (1986) 569.

[18] Z.L. Wang and J.M. Cowley, Ultramicroscopy 26 (1988) 233.

[19] Z.L. Wang, J. Liu and J.M. Cowley, Acta Cryst. A 45 (1989) 325.

[20] Y. Kim and T. Hsu, Surf. Sci. 275 (1992) 339.

[21] A. Hirata, K. Saiki, A. Koma and A. Ando, Surf. Sci. 319 (1994) 267.

[22] Y. Liang and D.A. Bonnell, Surf. Sci. 310 (1994) 128.

[23] Z.L. Wang and A. Howie, Surf. Sci. 226 (1990) 293.

[24] Z.L. Wang and J. Bentley, Ultramicroscopy 37 (1991) 103.

[25] Z.L. Wang, J. Microsc. 163 (1991) 261.

[26] Z.L. Wang and J. Zhang, Philos. Mag., submitted.